7-2011

THE COLLABORATIVE COLORADO–NEBRASKA UNMANNED AIRCRAFT SYSTEM EXPERIMENT

Adam L. Houston
University of Nebraska—Lincoln, ahouston2@unl.edu

Brian Argrow
University of Colorado-Boulder, Brian.Argrow@colorado.edu

Jack Elston
University of Colorado-Boulder

Jamie Lahowetz
University of Nebraska—Lincoln, jlahowetz2@unl.edu

Eric W. Frew
University of Colorado-Boulder

See next page for additional authors

Bulletin of the American Meteorological Society
Volume 93, Issue 1 (January 2012) pp. 39-54

THE COLLABORATIVE COLORADO–NEBRASKA UNMANNED AIRCRAFT SYSTEM EXPERIMENT

BY ADAM L. HOUSTON, BRIAN ARGROW, JACK ELSTON, JAMIE LAHOWETZ, ERIC W. FREW, AND PATRICK C. KENNEDY

Pioneering flights demonstrate the feasibility of using unmanned aircraft to collect in situ observations of mesoscale phenomena in the boundary layer within the U.S. National Airspace System.

Unmanned aircraft (UA) can provide observations of atmospherc phenomena that are either difficult or impossible to obtain with existing platforms. It is for this reason that facilitating the maturation of this relatively new technology has become a high priority in the atmospheric sciences. This position is reflected in the 2007 National Research Council Decadal Survey, which states that unmanned aircraft technology "should be increasingly factored into the nation's strategic plan for Earth science" (National Research Council 2007, p. 14). Moreover, the fiscal year 2008 budget for the National Oceanic and Atmospheric Administration (NOAA) featured an increased ▶

The NexSTAR unmanned aircraft on the catapult launcher during the 1 March 2009 deployment.

investment in unmanned aircraft systems (UAS[1]—that is, the aircraft along with the communications and logistics infrastructure required for their operation) to "evaluate the benefits and potential of using UAS" (NOAA 2008, p vi).

Many scientific applications of UAS require flights beyond the visual line of sight of the controller.[2] These operations require the versatility provided by increasing levels of autonomy in the UAS command and control architecture beyond that provided by the simple line-of-sight radio control used for model aircraft. A significant increase in system complexity is required to realize increased versatility/autonomy. Furthermore, observing mesoscale phenomena, particularly those that might be associated with precipitation, requires an ability to operate the UAS in high humidity and in the presence of strong aerodynamic forces. At a minimum, these conditions challenge the efficient operation of the UA and could compromise the flow of scientific and engineering data across the system. However, these conditions could also render the UA inoperable and unsafe. Managing the acute risk posed by the operation of UAS in the low levels of the atmosphere to observe mesoscale phenomena requires novel engineering solutions for 1) the communication between the multiple vehicles in the UAS, including the UA and both stationary and mobile ground-based vehicles; 2) the command and control of the aircraft; and 3) maintaining situational awareness in rapidly changing conditions.

UA autonomy not only introduces more system complexity but also elicits more scrutiny by airspace regulatory agencies, particularly for UAS operations in the lower atmosphere over land within the U.S. National Airspace System (NAS), since such operations are thought to pose an acute risk to other users of the NAS and persons or property on the ground. To our knowledge, only one prior project, the Atmospheric Radiation Measurement Unmanned Aerospace Vehicle (ARM-UAV) program (Stephens et al. 2000), utilized UAS to collect low-level observations over land in the NAS. These flights were conducted in the mid-1990s over the central United States (see Table 1). The regulatory environment has changed significantly since the mid-1990s and so, until the work discussed here, it remained unclear if UAS operations in the lower troposphere over land in the NAS were possible.

Therefore, while the potential utility of UAS for atmospheric science applications may be obvious, the engineering and regulatory hurdles that must be surmounted for their use are significant. These challenges motivated the Collaborative Colorado–Nebraska UAS Experiment

Table 1. Summary of previous autonomous UA operations.

Authors (year) Project name, year of Obs.	Location of Obs.	Aircraft name and specs.	Obs. over land	Obs. in the PBL	Obs. in the NAS	In situ Obs. of mesoscale phenomena
Stephens et al. (2000) ARM-UAV, **1994**	Oklahoma	Gnat-750 wingspan: 10 m Loaded wt: 1,140 lb	Yes	Yes	Yes	No
Schafer et al. (2001) Maritime Continent Thunderstorm Experiment, **1995**	Melville Island, Australia	Aerosonde wingspan: 2.9 m Loaded wt: ~30 lb	Yes	Yes	No	Yes (sea-breeze front)

[1] The terms *UA* and *UAS* are not interchangeable, since UA refers specifically to the airborne component of the UAS. The term *UAS* has been promulgated by the Department of Defense as a more robust term when referring to the operation of unmanned aircraft since the UA cannot function without the communication and logistics infrastructure system.

[2] Small aircraft cannot be easily spotted more than ~1–2 miles from the controller.

AFFILIATIONS: Houston and Lahowetz—Department of Earth and Atmospheric Sciences, University of Nebraska—Lincoln, Lincoln, Nebraska; Argrow, Elston, and Frew—Research and Engineering Center for Unmanned Vehicles, University of Colorado, Boulder, Colorado; Kennedy—Department of Atmospheric Science, Colorado State University, Fort Collins, Colorado
CORRESPONDING AUTHOR: Dr. Adam L. Houston, Department of Earth and Atmospheric Sciences, University of Nebraska—Lincoln, 214 Bessey Hall, Lincoln, NE 68588
E-mail: ahouston2@unl.edu

The abstract for this article can be found in this issue, following the table of contents.
DOI:10.1175/2011BAMS3073.1

In final form 27 July 2011

Holland et al. (2001) Port Hedland trial, **1998**	Port Hedland, Australia	Aerosonde wingspan: 2.9 m Loaded wt: ~30 lb	Yes	?	No	Yes (microburst)
Holland et al. (2001) **1999**	Off the coast of North Carolina	Aerosonde wingspan: 2.9 m Loaded wt: ~30 lb	No	Yes	Yes	Yes (precipitation band)
Soddell et al. (2004) Aerosonde Global Reconnaissance Facility Trials, **2000**	Southern Australia	Aerosonde wingspan: 2.9 m Loaded wt: ~30 lb	Yes	Yes	No	No
Watai et al. (2006) **2000**	Japan	Kite plane wingspan: 3 m Loaded wt: 35 lb	Yes	Yes	No	No
Curry et al. (2004) **2002**	Off the coast of Alaska	Aerosonde wingspan: 2.9 m Loaded wt: ~30 lb	No	Yes	Yes	No
Blakeslee et al. (2002) Mach et al. (2005) Altus Cumulus Electrification Study, **2002**	Florida Everglades	Altus-II wingspan: 17 m Loaded wt: 2,130 lb	Yes	No	Yes	No
Herwitz et al. (2004) **2002**	Kauai, Hawaii	Pathfinder-Plus wingspan: 36 m Loaded wt: 700 lb	Yes	No	Yes	No
Halverson et al. (2007) Tropical Cloud Systems and Processes Experiment, **2005**	Atlantic and Pacific Oceans	Aerosonde wingspan: 2.9 m Loaded wt: ~30 lb	No	Yes	No	No
Beven et al. (2008) NOAA tropical cyclone reconnaissance, **2005**	Atlantic Ocean	Aerosonde wingspan: 2.9 m Loaded wt: ~30 lb	No	Yes	No	Yes (tropical cyclone rainbands)
Lin (2006) **2005**	Pacific Ocean	Aerosonde wingspan: 2.9 m Loaded wt: ~30 lb	No	No	No	Yes (typhoon eyewall)
Ramanathan et al. (2007) Corrigan et al. (2006) Maldives Autonomous UAV Campaign, **2006**	Northern Indian Ocean	Manta wingspan: 2.7 m Loaded wt: ~25 lb	No	Yes	No	No
van den Kroonenberg et al. (2008) **2006/07**	Germany	Meteorological Mini UAV (M^2AV) wingspan: 2 m Loaded wt: 44 lb	Yes	Yes	No	No
Ambrosia et al. (2004) Wegener et al. (2008) Western States Fire Mission, **2007**	Western United States	Ikhana wingspan: 20 m Loaded wt: 10,500 lb	Yes	No	Yes	No

(CoCoNUE). The overarching objective of this collaborative project between the University of Colorado at Boulder and the University of Nebraska—Lincoln was to examine the feasibility of using a small UA operating semiautonomously to observe atmospheric phenomena within the terrestrial boundary layer of the NAS. To satisfy this objective, a field experiment was designed that utilized a UAS developed by the University of Colorado's Research and Engineering Center for Unmanned Vehicles (RECUV) to collect in situ data across airmass boundaries located over the Pawnee National Grassland (PNG) in northeast Colorado. The field phase of CoCoNUE was conducted on 1 March and 30 September 2009. During the 30 September operations, the UA was flown across both a cold front and thunderstorm-generated gust front. To our knowledge, the flights executed as part of CoCoNUE represent the first time that a UAS has been used to collect in situ observations of mesoscale phenomena in the lower atmosphere over land in the NAS.

PREVIOUS APPLICATION OF UAS IN THE ATMOSPHERIC SCIENCES. Since their earliest military applications, the UAS has been seen as an ideal platform for missions that are deemed too dull, dirty, or dangerous for manned aircraft. UAS that include small UA also benefit from flexibility in launch and landing, rapid deployability, and overall aerodynamic agility compared to manned aircraft. Such UAS characteristics are particularly well suited for a number of applications in the atmospheric sciences, especially ones involving mesoscale phenomena.

The earliest application of UAS in the atmospheric sciences documented in the formal literature was in the ARM-UAV program in the mid-1990s (Stephens et al. 2000; Table 1). Originally proposed in 1991 as part of the Atmospheric Remote Sensing and Assessment Program, ARM-UAV was responsible for several "firsts," including the first unescorted flight of a UA in class-A (controlled) airspace.

While observations were collected in the planetary boundary layer (PBL) during the ARM-UAV program, the principal focus was on the radiative processes within the mid/upper troposphere. Thus, the project required a large (>500 kg) UA capable of operating at high altitudes and for long deployments. Other notable projects such as the Altus Cumulus Electrification Study (ACES; Blakeslee et al. 2002; Mach et al. 2005) and the Western States Fire Mission (Ambrosia et al. 2004; Mach et al. 2005; Wegener et al. 2008) have also used large, high-altitude, long-endurance UA. The versatility of small UA (<25 kg takeoff weight) has been embraced by a number of investigators who require flexibility in launch and landing, rapid deployability, and reduced cost of operation, maintenance, and replacement compared to the large class of UA. The Aerosonde (Holland et al. 2001) is an example of a small UA that has been used extensively for atmospheric science research (Table 1). Other examples include the Manta used in the Maldives Autonomous UAV Campaign (Corrigan et al. 2006; Ramanathan et al. 2007) and the Meteorological Mini UAV used for turbulence measurements in Germany (van den Kroonenberg et al. 2008).

As noted in Table 1, many of the atmospheric science research projects utilizing UAS are conducted over the oceans (e.g., Holland et al. 2001; Curry et al. 2004; Corrigan et al. 2006; Lin 2006; Halverson et al. 2007; Beven et al. 2008), where the probability of encountering general aviation aircraft is low and the risk to people and property on the surface is nearly nonexistent. Of the projects that have been conducted over land, only the ARM-UAV project in the mid-1990s, ACES in 2002, the Kauai coffee plantation surveillance project in 2002 (Herwitz et al. 2004), and the Western States Fire Mission in 2007 have been conducted in the NAS. Operations over land in the NAS are notable because the policies for UAS operation in the NAS tend to be far more restrictive than those in other countries. Of these four projects conducted over land in the NAS, only the ARM-UAV operated in the lowest 1 km of the troposphere. This characteristic is significant because at these altitudes the margin for error is small and, as a consequence, obtaining authorization to conduct such flights is more difficult.

Prior to the execution of CoCoNUE, only a handful of projects had used UAS for data collection within *mesoscale* phenomena (e.g., Holland et al. 2001; Schafer et al. 2001; Lin 2006; Beven et al. 2008). Of these, only the Maritime Continent Thunderstorm Experiment (Schafer et al. 2001) and the Port Hedland trial (Holland et al. 2001) were conducted over land. However, both of these projects were carried out in Australia. Therefore, prior to CoCoNUE there is no recorded application of UAS to collect in situ observations of (low level) mesoscale phenomena over land in the NAS.

REGULATORY ENVIRONMENT. The Federal Aviation Administration (FAA) is tasked with ensuring that all aircraft in the NAS operate in a way that does not endanger other users of the NAS or persons or property on the ground. Kalinowski (2009, p. 3)

summarizes current FAA UAS policy by stating that "no person may operate a UAS in the National Airspace System without specific authority." "Specific authority" is required because UA are not compliant with portions of Title 14 of the Code of Federal Regulations and therefore "require an alternate means of compliance" (Davis 2008, p. 2). The type of authorization required to operate UAS is based on whether the aircraft will be operated as a model aircraft, civil aircraft, or public aircraft.

Guidelines for model aircraft operation are laid out in FAA Advisory Circular 91-57 (van Vuren 1981). Among these guidelines, model aircraft must be flown within visual line of sight of the operator and the aircraft must not exceed a ceiling of 400 ft. In addition, the directive UAS Interim Operational Approval Guidance 08-01 (Davis 2008, p. 10) provides guidance for dropping objects from UAS: "If the UA's intended operation includes the dropping or spraying of aircraft stores outside of active Restricted, Prohibited, or Warning Areas, the application must specifically address the hazard and make a clear case that injury to persons on the ground is extremely remote and operational risks have been sufficiently mitigated." The FAA also asserts that model aircraft "are not for business purposes" (see www.faa.gov/about/initiatives/uas/uas_faq/#Qn2).

Civil UA are those aircraft that are not used for recreation and are not owned or operated by the government. Civil applicants must apply for a Special Airworthiness Certificate—Experimental Category for UAS and Optionally Piloted Aircraft. An "airworthy" aircraft is defined in Section 3.5a of Title 14 of the Code of Federal Regulations (www.gpoaccess.gov/cfr/index.html) to be an aircraft that "conforms to its type design and is in a condition for safe operation." Further information on airworthiness and the process of certification can be found in FAA Order 8130.2G, Airworthiness Certification of Aircraft and Related Products. As stated in the Federal Register Notice (www.faa.gov/about/initiatives/uas/reg/media/frnotice_uas.pdf), Unmanned Aircraft Operations in the National Airspace System, "UAS issued experimental certificates may not be used for compensation or hire."

The operation of UAS owned by the U.S. government, state governments, and agencies is considered "public use." For UAS operating as public aircraft, the authority is the Certificate of Authorization or Waiver (COA). Current policies for the COA are outlined by Davis (2008) and Kalinowski (2009). The COA application requires an airworthiness statement and the contingency procedures that will be executed for many possible equipment malfunctions or emergencies. Authorization is given for a single aircraft and single geographic region.

As a government-sponsored project executed by the Universities of Colorado and Nebraska, UAS operations for CoCoNUE were public operations and therefore required a COA. COA 2008-WSA-51 was granted by the FAA for the Hobbico NexSTAR airframe to be operated within coordinate boundaries located in the Pawnee National Grassland (see Fig. 1b for the region covered by the COA). For CoCoNUE and similar projects, the FAA mandates the following for UAS operation:

- The UA must remain within visual contact of an observer (ground based in this experiment) at all times. The nominal separation between the UA and the observer is 1 mi horizontally and 1,000 ft vertically. This is required to enable deconfliction if other aircraft enter the nearby airspace.
- A Notice to Airmen (NOTAM) is a sufficient mechanism for notifying pilots of impending operations.
- It is necessary to maintain the ability to communicate with local air traffic control and manned aircraft (in this case, through a hand-held aviation radio).

THE UNMANNED AIRCRAFT SYSTEM.

The NexSTAR unmanned aircraft. The choice of aircraft was principally guided by the need to target transient mesoscale phenomena. The scale of such phenomena—typically O(10 km)—constrains the cruising speed and endurance of the aircraft. The transience and variability of mesoscale phenomena require an aircraft that is rapidly deployable and redeployable and therefore constrain the aircraft size. The maximum anticipated sustained winds dictate the aircraft's maximum air speed.

The NexSTAR UA was chosen for this work (Fig. 2). The NexSTAR airframe is the low-cost, almost-ready-to-fly kit produced by Hobbico. It is composed of balsa and plywood covered with a thin Monokote plastic film. It is lightweight (5.21 kg take off weight) and small (wingspan of 1.7 m) and is therefore easily transportable. It is also small enough to use in a relatively simple catapult launching system (Fig. 2). The catapult uses an aluminum rail to guide the aircraft while it is accelerated forward using rubber tubing. This system can be set up and taken down in minutes.

Mesoscale phenomena that are O(10 km) in size cannot be reliably sampled with UA operating

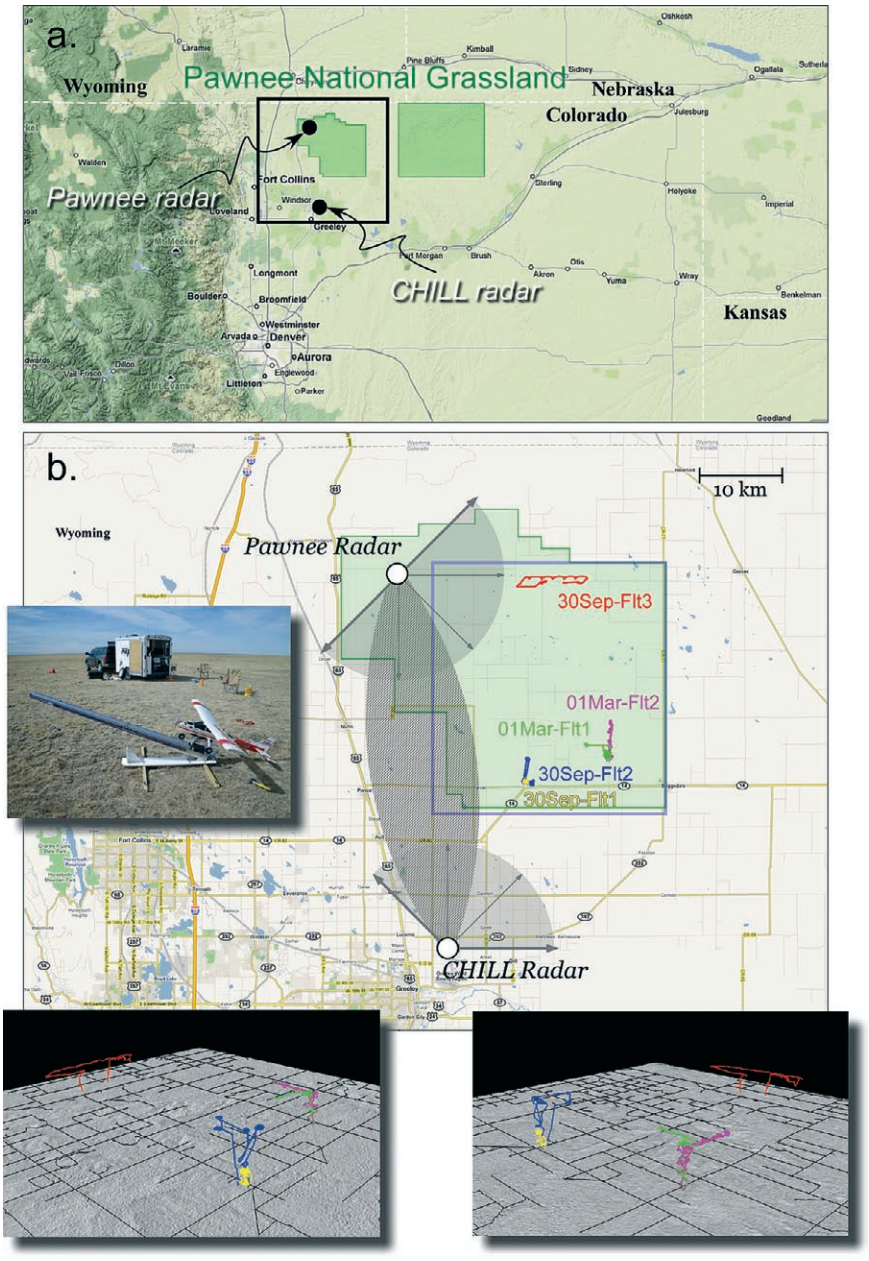

Fig. 1. (a) Location of Pawnee National Grassland and CSU-CHILL/Pawnee radars in northeast Colorado. (Background map courtesy of Google Maps.) (b) Summary of flights conducted on 1 Mar and 30 Sep 2009 [map area occupies the region in (a) bounded by the black rectangle]. The locations of the CSU radars are also illustrated along with the azimuth angles composing the scanning sectors for each radar (in semitransparent gray), while the hatched region represents the region too close to the baseline to allow for reliable dual-Doppler measurements. The boundaries of COA 2008-WSA-51 are illustrated with a blue box. The NexSTAR on the catapult and the mobile ground station are illustrated in the upper shadowed panel, and 3D renderings of the trajectories for each flight are illustrated in the two bottom shadowed panels (the perspectives are toward the northeast in the left panel and toward the northwest in the right panel).

via line-of-sight (nonautonomous) command and control. Thus, sampling such phenomena requires semiautonomous operations. The Piccolo autopilot manufactured by Cloud Cap Technologies is used onboard the NexSTAR for "low level" flight control (i.e., instructions to ensure stable flight, waypoint navigation, etc.). The autopilot utilizes an onboard GPS sensor to navigate the aircraft to waypoint positions that can be changed during the flight.

Although small UA such as the NexSTAR provide versatility in launch, landing, and transport, their small maximum payloads (~0.5 kg for the NexSTAR) limit the amount of instrumentation that can be carried on board. However, for missions focused on collecting observations of temperature, moisture, pressure, and wind velocity, the scientific instrumentation generally contributes very little to the overall payload. This is particularly true of the sensors used on the NexSTAR. The NexSTAR has also been outfitted with a pressure, temperature, and humidity sonde originally developed for use in the Miniature In-situ Sounding Technology (MIST) dropsonde designed by the In-Situ Sensing Facility at the National Center for Atmospheric Research's (NCAR's) Earth Observing Laboratory. This sonde is based on the Vaisala RS92 core. (The specifications of the RS92 sonde appear in Table 2. For more information on the RS92 sonde, see www.vaisala.com/en/products/soundingsystemsandradiosondes/radiosondes/Pages/RS92.aspx. For more information on the MIST sonde, see www.eol.ucar.edu/development/avaps-iii/documentation/miniture-

Fig. 2. The NexSTAR UA on the catapult prior to launch on 1 Mar 2009.

in-situ-sounding-technology.) Flight-level winds are calculated in real time using the Piccolo autopilot's proprietary algorithm based on the air velocity and ground velocity of the aircraft. The meteorological data collected by the aircraft are transmitted in real time to the mobile ground station via a 2.4-GHz (Wi-Fi) data link and are recorded on board the UA as well.

The rapid redeployment of the aircraft not only requires the ability to rapidly launch but also the ability to rapidly and safely "refuel" following the previous deployment. To this end, the NexSTAR is outfitted with an electric motor powered by an easily exchangeable battery pack. With this propulsion system, the NexSTAR cruises with a true air speed of ~20 m s^{-1} at ~75% throttle and an endurance of ~45 minutes, enabling flights of as much as 54 km. The engine can produce a top air speed of ~35 m s^{-1}, which was deemed sufficient for the mesoscale phenomena of interest. The aircraft can easily reach the maximum altitude allowed by the COA (1,000 ft); the aircraft's actual ceiling is unknown, since operations above 1,000 ft are prohibited.

Electronic tethering and ground-based support vehicles. The Piccolo autopilot used for the semiautonomous operation of the UAS during CoCoNUE requires a GPS waypoint or series of waypoints to direct the UA. These waypoints can be communicated to the autopilot in real time, allowing for a dynamic flight path. In CoCoNUE, instead of manually setting waypoints ahead of the UA, the onboard flight computer was used to track a mobile, ground-based vehicle (tracker) by utilizing GPS data sent over the ad hoc Wi-Fi network. This capability is enabled through the Networked UAS Command, Control, and Communication (NetUASC3) software developed by RECUV. This software resides at the application layer of each networked node used in the system and provides service discovery and a publish/subscribe architecture. This allows for dynamic reconfiguration of the system and the ability to generate higher-level tasks, such as "track this ground vehicle using its GPS information" (Elston et al. 2009).

This navigation strategy, termed *electronic tethering*, has two principal benefits. First, targeting/navigation decisions made by the meteorologist in command need to be communicated to the tracker only, instead of both the tracker and the UA. Second, this strategy facilitates compliance with the FAA requirement that the UA must remain in visual line of sight of an observer at all times. In CoCoNUE, the UA was flown beyond the visual line of sight of the ground station and thus mobile observers were required. Therefore, not only does the telemetry of the tracker guide the UA but the personnel within the tracker can maintain constant visual contact with the UA.

To maintain the ability to observe both the aircraft and the surrounding airspace, observers in the tracker must have a means of seeing directly above them.[3] To facilitate this, a Ford Edge with a panoramic sunroof was employed. With this functionality, observers in

[3] This capability was not available during the flights of 1 March and as a consequence severely limited the efficiency of operations (the tracker had to stop repeatedly in order to regain visual contact).

Table 2. Specifications of the sensors composing the Vaisala RS92 sonde that has been integrated into the MIST sonde used on the NexSTAR UA (based on a datasheet available online at www.vaisala.com/en/products/soundingsystemsandradiosondes/radiosondes/Pages/RS92.aspx).

	Response time	Resolution	Accuracy
Temperature	<0.4 s	0.1°C	0.5°C
Relative humidity	<0.5 s	1%	5%
Pressure	N/A	0.1 hPa	1 hPa

Fig. 3. The RMGS.

the tracker could maintain an uninterrupted view of the UA at all times.

The RECUV Mobile Ground Station (RMGS; Fig. 3) served as the base of operations during CoCoNUE. The RMGS is a 10 ft × 6 ft × 8 ft trailer designed to transport and support the UAS and contains a full complement of support tools, a weather station, and computers running the NetUASC3 software for situational awareness and UAS control.

Required personnel. A minimum of six personnel was required for the safe operation of the UAS in compliance with FAA regulations during CoCoNUE. These personnel occupied eight positions on the team:

1) Pilot in command
2) Meteorologist in command
3) Pilot at control for semiautonomous operations
4) Pilot at control for manual operations
5) Tracker driver
6) Tracker navigator
7) UA spotter
8) Airspace observer

The pilot in command has the final authority and responsibility for the operation and safety of the flight. The meteorologist in command is responsible for making tactical decisions based on meteorological data. The pilot at control for semiautonomous operations is in charge of monitoring UA status, issuing high-level commands, and changing mission-level parameters of the UA. The pilot at control for manual operations is in charge of controlling the UA manually during takeoff and landing over the 900-MHz control link. During CoCoNUE the pilots were located at the RMGS (one person served as both the pilot in command and pilot at control for manual operations). Thus, the UA was operated beyond the visual line of sight of the personnel with the capability of controlling the aircraft. The meteorologist in command was located at the RMGS for the 1 March operations and in the tracker for the 30 September operations. The tracker was populated with a dedicated driver, a navigator (or the meteorologist in command), a UA spotter, and an airspace observer. The airspace observer was responsible for surveying the surrounding airspace for other aircraft.

EXPERIMENT DESIGN. *Mesoscale targets.* Airmass boundaries were chosen as the mesoscale phenomenon to target in CoCoNUE. Not only are airmass boundaries (e.g., cold fronts, warm fronts, drylines, and thunderstorm outflow boundaries) ubiquitous, but they are also characterized by an across-boundary scale on the order of 1–10 km that can be easily sampled by UAS without requiring flight times at the limit of many small UA capabilities. This across-boundary scale also has the benefit of yielding a clear signal in the in situ thermodynamic and kinematic data that would be collected by the UAS. Despite the small across-boundary scale, many airmass boundaries are characterized by along-boundary scales on the order of hundreds to thousands of kilometers. Therefore, airmass boundaries have the advantage of being easily trackable via the existing network of synoptic-scale observations and, consequently, also forecastable well in advance of planned UAS operations. Furthermore, airmass boundaries are readily apparent in radar reflectivity and velocity data during the late spring, summer, and early fall through the combination of biological targets and Bragg scattering (Wilson et al. 1994).

Airmass boundaries are not only relatively easy to target; there is also substantial evidence that they can have a significant impact on a number of mesoscale processes/phenomena: for example, deep convection initiation [refer to the review of Weckwerth and Parsons (2006)], deep convection maintenance/propagation (e.g., Newton 1963; Weaver 1979; Weaver and Nelson 1982; Wilhelmson and Chen 1982; Atkins et al. 1999; Houston and Wilhelmson 2007a, 2012),

and tornadogenesis (e.g., Purdom 1976; Maddox et al. 1980; Simpson et al. 1986; Wilson and Schreiber 1986; Purdom 1993; Lee and Wilhelmson 1997; Markowski et al. 1998; Rasmussen et al. 2000; Caruso and Davies 2005; Houston and Wilhelmson 2007b), among many others. However, to understand the impact of airmass boundaries on these processes/phenomena requires data that UAS can, perhaps uniquely, collect.

Area of operations. CoCoNUE was conducted in the western half of the Pawnee National Grassland located in northeast Colorado (Fig. 1a). The Pawnee National Grassland was selected principally because its modest population density obviates the need to operate over major urban areas and because of its proximity to the Colorado State University–University of Chicago–Illinois State Water Survey (CSU-CHILL)/Pawnee radars (Brunkow et al. 2000; Fig. 1). The ability to operate over a low-population-density area made it easier to receive FAA authorization. The proximity to the CSU-CHILL/Pawnee radars yielded meteorological data that could be used in real time for targeting decisions and enabled ex post facto dual-Doppler synthesis for comparison of the derived two-dimensional wind field to the in situ observations collected by the UAS. The PNG is also characterized by well-maintained (gravel) roads that the ground-based observers can travel along to maintain visual tracking of the UA for FAA compliance.

Decision support system. During autonomous operations, in situ meteorological data collected by the UAS, tracker and UA telemetries, and UA aeronautical data are displayed at the RMGS through the graphical user interface (GUI) of the NetUASC3 software (Fig. 4a). The GUI also has the capability to underlay a variety of maps along with georeferenced images of meteorological data. The NetUASC3 GUI provides the pilot at control for semiautonomous operations with interfaces to adjust mission parameters and issue high-level commands.

Situational awareness during CoCoNUE relied on real-time Doppler radar data from the CSU-CHILL/Pawnee radars. These radars are positioned to enable volumetric data collection over the PNG at altitudes that sufficiently represent the planetary boundary layer. The CSU-CHILL staff set up a real-time feed of both the CHILL and Pawnee radar data converted to level II format and optimized to limit the bandwidth required for dissemination. The CHILL and Pawnee radars were configured for a 3.5-min synchronized volume scan that allowed for ex post facto dual-Doppler synthesis. Additional real-time meteorological data were also made available for situational awareness. These data included 1-km visible satellite images and Automated Surface Observing System (ASOS) observations and were served through the Unidata Internet Data Distribution via the University of Nebraska.

The Gibson Ridge Radar and UAS Visualization Interface (GRRUVI) was the primary tool for integrating radar data, supplemental meteorological data, UA and tracker telemetries, and road networks necessary to maintain situational awareness. GRRUVI uses the GIS-driven Gibson Ridge level II (GR2; www.grlevelx.com/grlevel2/) data viewer (Fig. 4b). GRRUVI also provides an interface for communication between the tracker navigator and spotters and

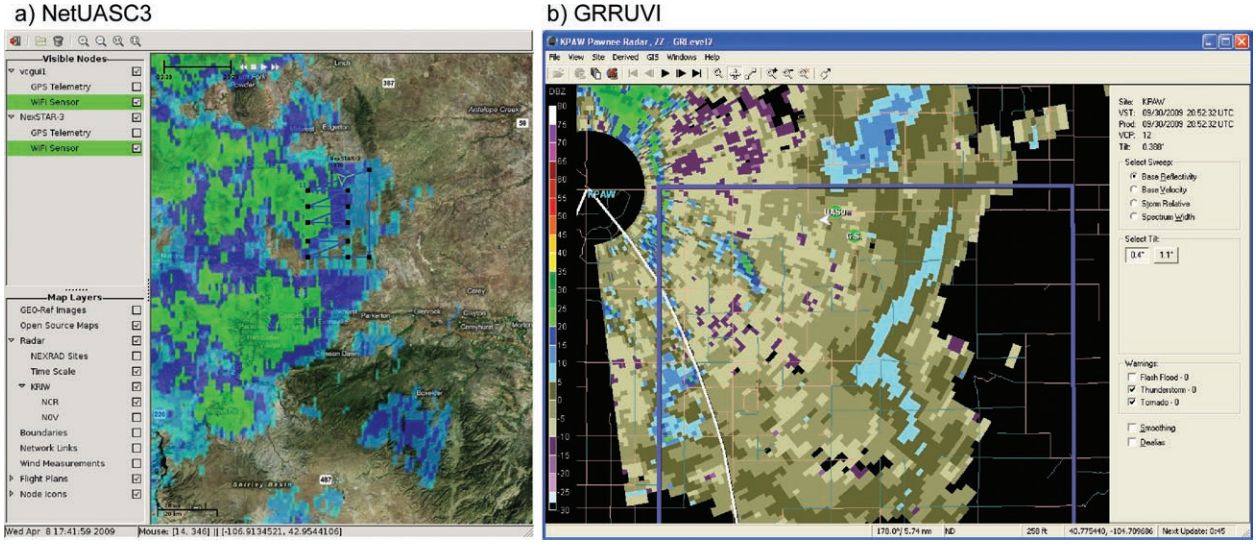

Fig. 4. (a) NetUASC3; and (b) GRRUVI GUIs.

Table 3. Summary of CoCoNUE flights.				
Date and flight	**Launch/landing (UTC) Flight time (minutes)**	**Altitude (m) starting/maximum (MSL) Maximum (AGL)**	**Ground station location (°N, °W)**	**Maximum distance from GS (km)**
01Mar-Flt1	19:48/20:11 24	1,495/1,811 316	40.660, −104.411	3.4
01Mar-Flt2	18:49/19:15 26	1,495/1,811 316	40.660, −104.411	4.5
30Sep-Flt1	18:12/18:23 11	1,510/1,655 135	40.644, −104.525	0.6
30Sep-Flt2	18:49/19:15 26	1,509/1,933 424	40.644, −104.525	2.9
30Sep-Flt3	20:45/21:16 31	1,593/1,858 265	40.855, −104.504	5.3

the RMGS using the Internet Relay Chat protocol as well as a mechanism for broadcasting the telemetry of each ground-based vehicle to anyone running GRRUVI.

Transfer of situational awareness data and communication via the chat interface relied on the (Verizon) evolution-data only/evolution-data optimized (EVDO) (broadband cellular) network in place over the PNG. For purposes of redundancy, direct radio communication was employed between the RMGS and the tracker and between the RMGS and the CSU radar operators.

RESULTS. The FAA issued COA 2008-WSA-51 on 9 February 2009 authorizing flights by the NexSTAR over nearly the entire western half of the PNG (Fig. 1b). CoCoNUE was executed in two days of operations (Table 3). Two flights were executed on 1 March 2009 and three flights were executed on 30 September 2009. The first two flights of 30 September (30Sep-Flt1 and 30Sep-Flt2) targeted coherent boundary layer circulations manifested as linear signatures in CHILL radar data but were terminated prematurely because of problems with the electronic tether. The third flight (30Sep-Flt3) targeted two airmass boundaries traveling southeastward across the PNG. This flight is the focus of the analysis presented below.

The preliminary target for the 30 September operations was a cold front that was projected

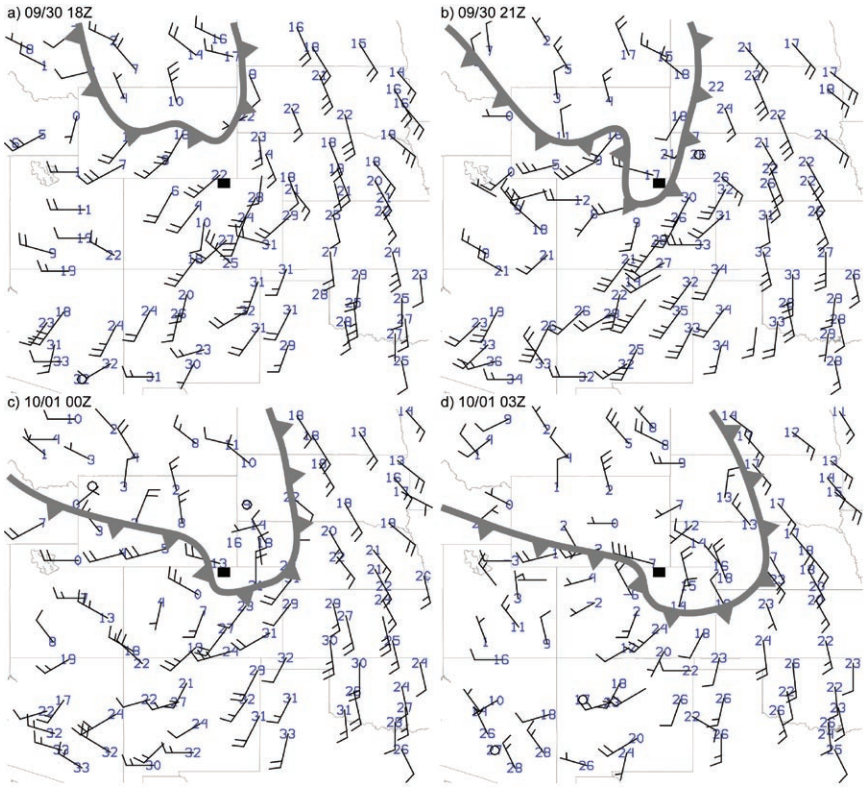

Fig. 5. Progression of the cold front at (a) 1800 and (b) 2100 UTC 30 Sep 2009 and (c) 0000 and (d) 0300 UTC 1 Oct 2009. The 10-m winds and 2-m temperature (°C) are also illustrated along with the frontal position. The black rectangle is the location of the operations area.

to move across the PNG. Thunderstorm-generated gust fronts were to serve as a backup target should the front either not present itself in the radar data or pass through the PNG after dark (COA 2008-WSA-51 required UAS operations to be completed prior to sunset). A summary of the evolution of the front during the day and early evening appears in Fig. 5.

The cold front was identified in the Pawnee radar data at ~20:28 UTC (all times are reported in UTC). The RMGS was redeployed from its location for 30Sep-Flt2 to a position 23 km north (Fig. 1b). The UA was launched from the RMGS at 20:45 just as the cold front passed. The aircraft ascended to an altitude of 1,858 m MSL (265 m above the height of the RMGS) as it crossed the cold front and entered the cooler and moister air mass west of the front. The UA traveled westward for an additional 3 km before returning eastward 8 km. Shortly after the UA began its westward return to the RMGS, it transected a gust front traveling east-southeastward within the postfrontal air mass. The total flight time was 31 minutes.

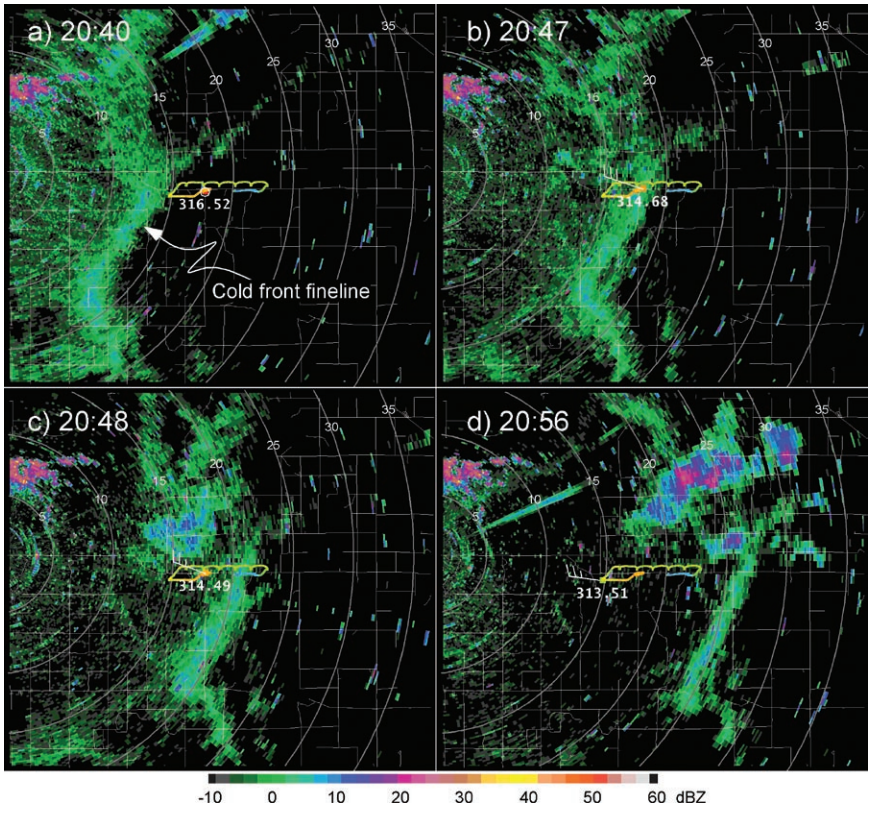

Fig. 6. UA trajectory for 30Sep-Flt3 along with the radar reflectivity from the Pawnee radar at an elevation angle of 1.2° and instantaneous UA observations of wind velocity [staff and barb; half (full) barb represents 2.5 (5.0) m s^{-1}] and potential temperature (K) at (a) 20:40, (b) 20:47, (c) 20:48, and (d) 20:56 UTC. Range rings are contoured every 5 km.

An illustration of the UA track (colored according to potential temperature; warm colors correspond to warm temperatures) overlying the radar reflectivity data from the Pawnee radar is illustrated in Fig. 6. The UA was launched just as the radar fineline associated with the cold front reached the RMGS. The boundary-relative distributions of water vapor mixing ratio and potential temperature collected by the UA (Fig. 7) reveal a very distinct increase in moisture and drop in temperature shortly after launch. This signal is ostensibly the cold front; however, because the UA was ascending at the time, the observed signal may also be a consequence of the UA leaving a shallow superadiabatic layer. As evidenced in the prefrontal vertical profiles of potential temperature collected in the descending segment of 30Sep-Flt1 and ascending segment of 30Sep-Flt2[4] along with the postfrontal vertical profile collected in the descending segment of 30Sep-Flt3 (Fig. 8a), a superadiabatic layer is indeed present on either side of the front. However, this layer is less than 10 m thick. Thus, for 30Sep-Flt3, the decrease in potential temperature above this shallow layer should be wholly attributable to the cold front. Moreover, the water vapor mixing ratio profile for the ascending segment of 30Sep-Flt3 (Fig. 8b) reveals a rather sudden increase from ~3.3 to ~3.7 g kg^{-1} as the UA traveled above ~40 m AGL. This increase is not reflected in any of the other profiles collected. Therefore, it appears that the drop in potential temperature and increase in water vapor mixing ratio apparent in Fig. 7 near the time of fineline passage is attributable to the cold front.

Wind observations collected by the UAS during 30Sep-Flt3[5] generally agree with the dual-Doppler-

[4] The temperature and moisture observations in the lowest levels of both the descending profile from Flt1 and ascending profile from Flt2 did not pass quality control and so these soundings are not included in the analysis.

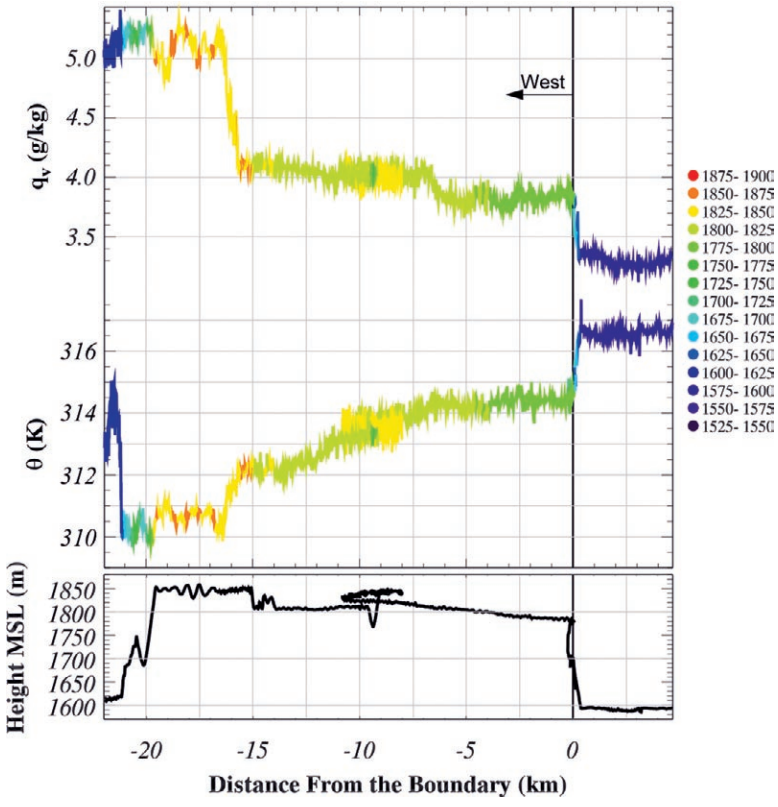

Fig. 7. Boundary-relative distribution of water vapor mixing ratio (top series; g kg^{-1}), potential temperature (middle series; K), and UA height (bottom series; m MSL) for 30Sep-Flt3. Water vapor mixing ratio and potential temperature are colored according to UA height.

derived winds calculated near the flight level (Fig. 9): differences in wind speed are typically less than ±25% and wind direction differences are typically less than 15°. Differences are largest for UA positions farthest from dual-Doppler data points (e.g., 21:13 in Fig. 9 for which the lateral separation, Δx, is 1,452.3 m). The correlation between relative speed errors (direction errors) and the lateral separation between the UA and the nearest dual-Doppler data point is 0.85 (0.80). Spatial separation between UA positions and dual-Doppler data points is principally dictated by the availability of radar returns near the UA. In this comparison, no dual-Doppler data more than 500 m vertically and 2000 m horizontally

[5] Only 30Sep-Flt3 could be used to conduct the comparison, since clear-air scatterers were insufficient to yield clear-air velocity data during the 1 March flights and the radars were down during the first two flights of the 30 September operations.

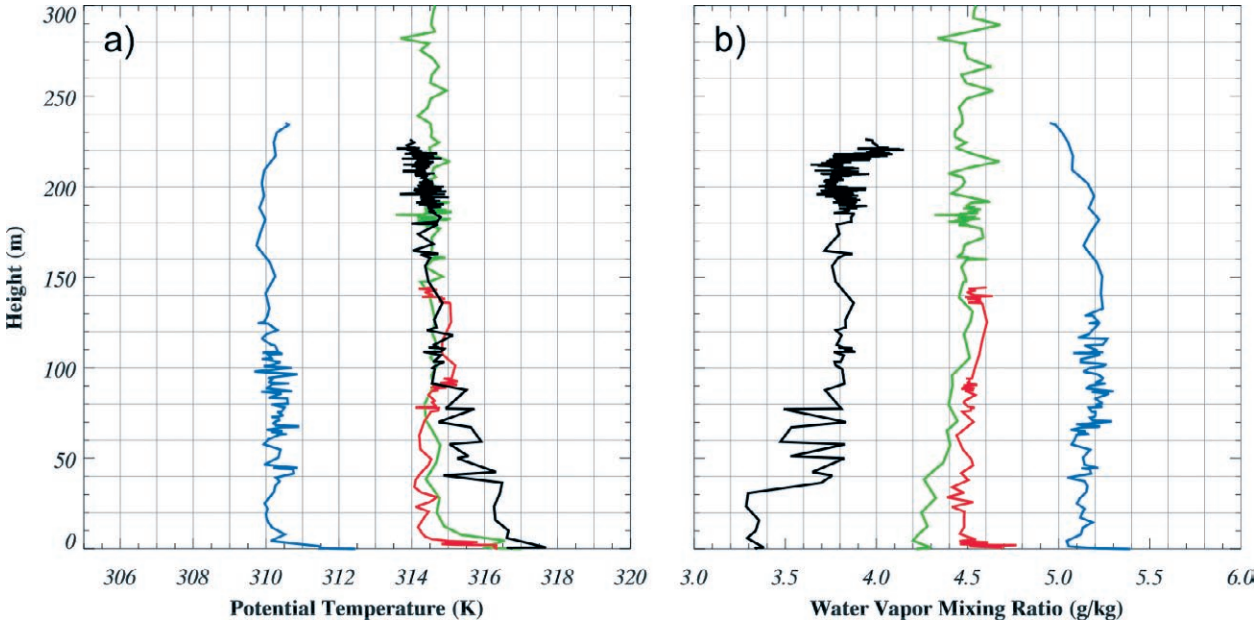

Fig. 8. Vertical profiles of (a) potential temperature (K) and (b) water vapor mixing ratio (g kg^{-1}) derived from UA ascents during takeoff and descents at landing. Black curves represent the data collected during the ascent of 30Sep-Flt3, blue curves are for the (postfrontal) descent of 30Sep-Flt3, green curves are for the (prefrontal) ascent of 30Sep-Flt2, and the red curves are for the (prefrontal) descent of 30Sep-Flt1.

Fig. 9. Differences between the UA-observed and dual-Doppler-derived wind. (a) Time series of the relative difference (black trace; data points are colored to match the position on the UA trajectory illustrated above the panel), UAS wind (blue staff and barbs following typical meteorological conventions), dual-Doppler wind (green staff and barb), and lateral (Δx) and vertical (Δz) separations between the UA position and the nearest dual-Doppler wind value. (b) Time series of wind direction differences.

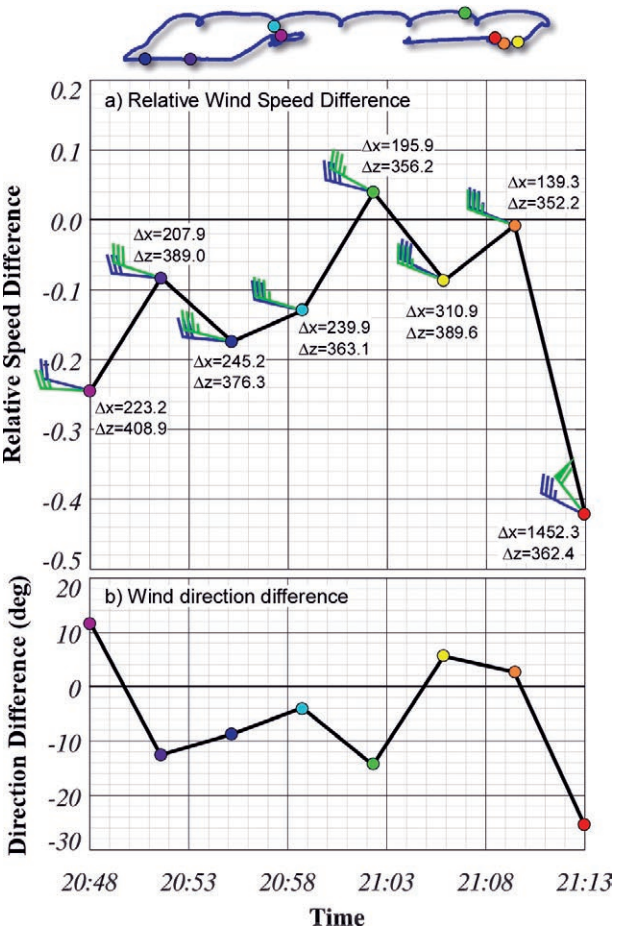

from the UA position were included in the data comparison. Gridded dual-Doppler data were interpolated to the UA point using a single-pass adaptive Barnes scheme (Askelson et al. 2000) with a lateral radius of influence of 1,000 m and a vertical radius of influence of 250 m. A 60-s running centered average was applied to UA data prior to interpolation.

While collecting measurements in the postfrontal air mass, the UA transected a gust front that appears to have originated from precipitation over southern Wyoming. Figure 10 reveals the relationship between the subtle fineline associated with this gust front and the increase in water vapor mixing ratio across the boundary. This behavior in the moisture field, along with the change in potential temperature across the boundary, is also illustrated in the cold front–relative profiles in Fig. 7 (the UA encountered the gust front 15.5 km west of the cold front). The gust front is also reflected in the wind field sampled by the UA (Figs. 10 and 11). Winds are found to back from ~300° ahead of the gust front to 285° at the boundary to 260°–270°

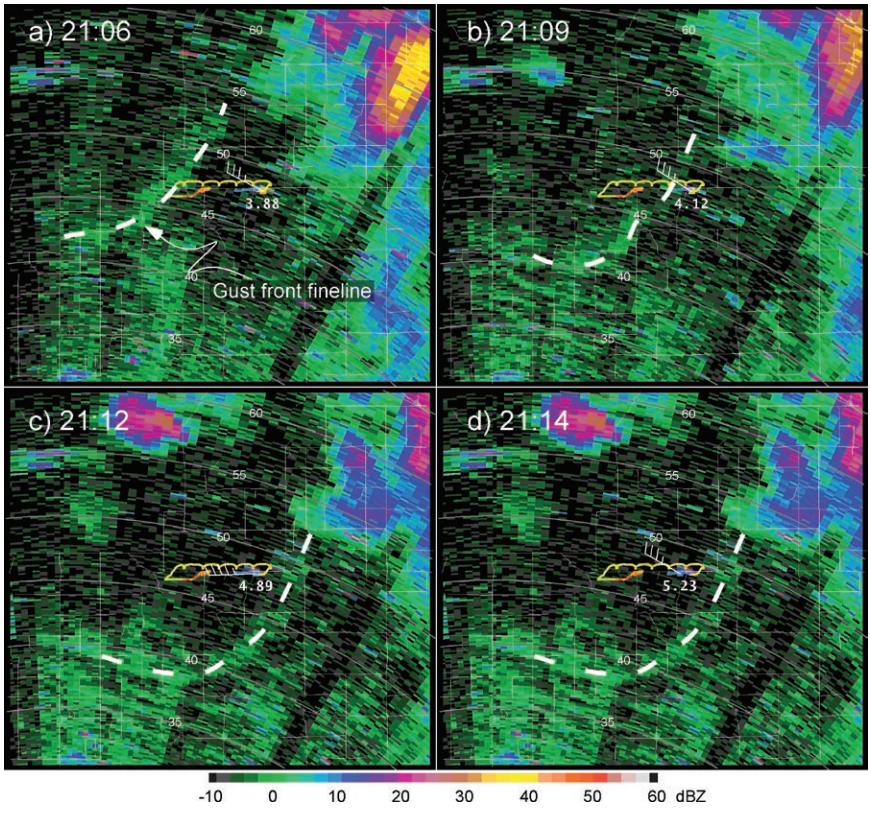

Fig. 10. UA trajectory for 30Sep-Flt3 along with the radar reflectivity from the CHILL radar at an elevation angle of 0.7° and instantaneous UA observations of wind velocity [staff and barb; half (full) barb represents 2.5 (5.0) m s^{-1}] and water vapor mixing ratio (g kg^{-1}) at (a) 21:06, (b) 21:09, (c) 21:12, and (d) 21:14 UTC. The location of the fineline associated with the gust front is annotated with broken curve. Range rings are contoured every 5 km.

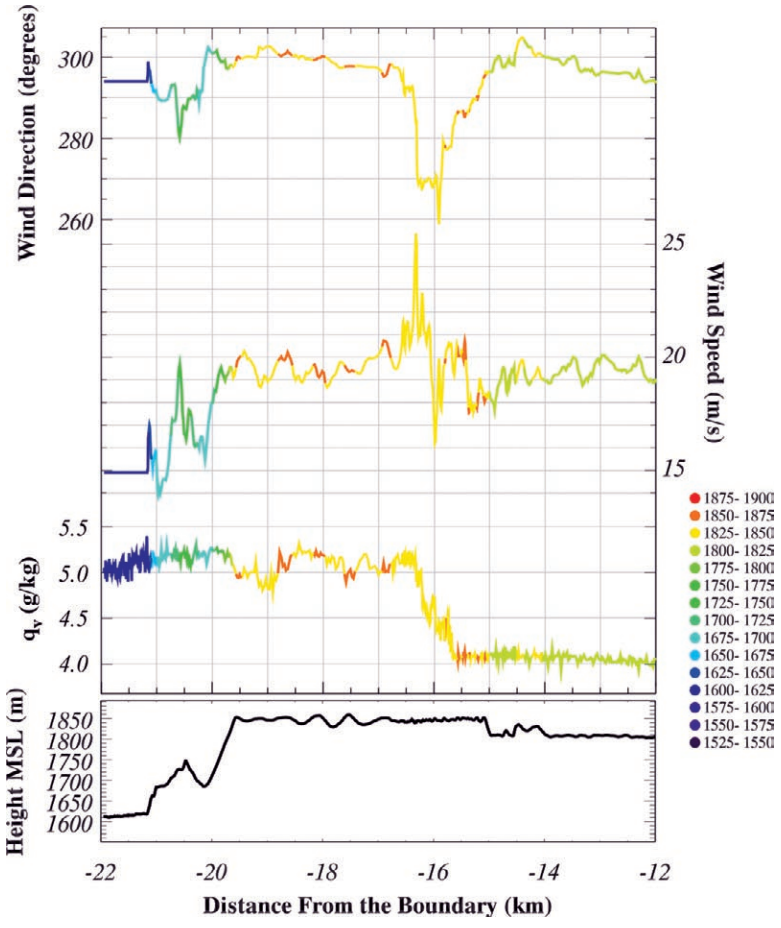

Fig. 11. Boundary-relative distribution of wind direction (top series; °), wind speed (top middle series; m s^{-1}), water vapor mixing ratio (bottom middle series; g kg^{-1}), and UA height (bottom series; m MSL) for 30Sep-Flt3. Wind direction, wind speed, and water vapor mixing ratio are colored according to UA height.

within the frontal transition zone. Wind speeds exhibited coherent fluctuations across the boundary, with speeds as small as 14 m s^{-1} within the frontal transition zone to speeds as large as 25.5 m s^{-1} just west of the transition zone.

SUMMARY. The complicated marriage of engineering, meteorology, and regulatory policy involved in using unmanned aircraft to observe atmospheric phenomena in the terrestrial boundary layer within the National Airspace System has meant that the feasibility of this endeavor has been difficult to determine. This has been particularly true for atmospheric phenomena that require UAS to operate with some level of autonomy. The UAS and experiment design solution presented here offers an FAA-compliant strategy for using a semiautonomous UAS to collect data in low-level, terrestrial, mesoscale phenomena within the NAS. The execution of CoCoNUE demonstrated that the operation of UAS in this manner is not only possible but also has the potential to reveal important characteristics of mesoscale phenomena that are difficult or impossible to sample in any other way. These kinds of observations are essential to answering heretofore unanswerable questions regarding such phenomena. Moreover, this project revealed that an open, nonadversarial relationship with the FAA not only works to the advantage of atmospheric scientists wishing to use UAS for such missions but also helps to move the entire endeavor of using UAS for science and engineering toward a future in which UAS operation in the NAS is safe, easy, and ubiquitous. This project was only a single step toward that end. The University of Colorado and the University of Nebraska continue to use the lessons learned in CoCoNUE to develop UAS that are designed to observe low-level mesoscale phenomena and to work with the FAA to integrate these UAS into the NAS (e.g., Elston et al. 2011).

ACKNOWLEDGMENTS. The authors wish to thank E. Rasmussen and an anonymous reviewer whose critique of this manuscript led to an improved final product. Funding for this work was provided through NSF Grants ATM-0715941, ATM-0715875, ATM-0800763, and ATM-0824160. The initial collaboration between the University of Nebraska and the University of Colorado was supported by a Big 12 Faculty Fellowship awarded to A. Houston. Thanks go to Paul Hein and Jim George at CSU-CHILL for setting up the real-time feed of radar data. Thanks also go to the rest of the support staff at the CSU-CHILL facility for assisting the project during operations. We are grateful to Terry Hock and Dean Lauritsen at the In-Situ Sensing Facility at NCAR's Earth Observing Laboratory for providing the MIST sonde, reprogramming the sensor board to enable third-party use, and offering guidance regarding optimal installation locations on the UA. We would also like to thank the CoCoNUE participants: Eric Frew, Cory Dixon, Maciej Stachura, Jason Durrie, Anthony Carfang, and Anthony Reinhart.

REFERENCES

Ambrosia, V. G., S. S. Wegener, J. A. Brass, and S. M. Schoenung, 2004: The UAV Western States Fire Mission: Concepts, plans and developmental advancements. Preprints, *Third AIAA "Unmanned Unlimited" Conf., Workshop, and Exhibit*, Chicago, IL, American Institute for Aeronautics and Astronautics, AIAA-2004-6415.

Askelson, M. A., J.-P. Aubagnac, and J. M. Straka, 2000: An adaptation of the Barnes filter applied to the objective analysis of radar data. *Mon. Wea. Rev.,* **128,** 3050–3082.

Atkins, N. T., M. L. Weisman, and L. J. Wicker, 1999: The influence of preexisting boundaries on supercell evolution. *Mon. Wea. Rev.,* **127,** 2910–2927.

Beven, J. L., II, and Coauthors, 2008: Annual summary: Atlantic hurricane season of 2005. *Mon. Wea. Rev.,* **136,** 1109–1173.

Blakeslee, R. J., D. Mach, M., M. D. Desch, R. A. Goldberg, W. M. Farrell, and J. G. Houser, 2002: The Altus Cumulus Electrification Study (ACES): A UAV-based science demonstration. Preprints, *First Tech. Conf. and Workshop on Unmanned Aerospace Vehicles, Systems, Technologies, and Operations*, Portsmouth, VA, American Institute for Aeronautics and Astronautics, Paper AIAA-2002-3405.

Brunkow, D., V. N. Bringi, P. C. Kennedy, S. A. Rutledge, V. Chandrasekar, E. A. Mueller, and R. K. Bowie, 2000: A description of the CSU–CHILL National Radar Facility. *J. Atmos. Oceanic Technol.,* **17,** 1596–1608.

Caruso, J. M., and J. M. Davies, 2005: Tornadoes in non-mesocyclone environments with pre-existing vertical vorticity along convergence boundaries. *Electronic Journal of Operational Meteorology, 2004.* [Available online at www.nwas.org/ej/index.php.]

Corrigan, C., V. Ramanathan, M. V. Ramana, D. Kim, and G. Roberts, 2006: Chasing black carbon using autonomous unmanned aerial vehicles. *Eos, Trans. Amer. Geophys. Union,* **87** (Fall Meeting Suppl.), Abstract A43A-0106.

Curry, J. A., J. Maslanik, G. J. Holland, and J. Pinto, 2004: Applications of aerosondes in the Arctic. *Bull. Amer. Meteor. Soc.,* **85,** 1855–1861.

Davis, K. D., 2008: Interim Operational Approval Guidance 08-01: Unmanned aircraft systems operations in the U.S. National Airspace System. Aviation Safety Unmanned Aircraft Program Office Rep. AIR-160, 18 pp.

Elston, J., E. W. Frew, D. Lawrence, P. Gray, and B. Argrow, 2009: Net-centric communication and control for a heterogeneous unmanned aircraft system. *J. Intell. Rob. Syst.,* **56,** 199–232.

——, J. Roadman, M. Stachura, B. Argrow, A. L. Houston, and E. W. Frew, 2011: The Tempest unmanned aircraft system for in situ observations of tornadic supercells: Design and VORTEX2 flight results. *J. Field Rob.,* **28,** 461–483.

Halverson, J. B., and Coauthors, 2007: NASA's Tropical Cloud Systems and Processes Experiment: Investigating tropical cyclogenesis and hurricane intensity change. *Bull. Amer. Meteor. Soc.,* **88,** 867–882.

Herwitz, S. R., and Coauthors, 2004: Imaging from an unmanned aerial vehicle: Agricultural surveillance and decision support. *Comput. Electron. Agric.,* **44,** 49–61.

Holland, G. J., and Coauthors, 2001: The Aerosonde robotic aircraft: A new paradigm for environmental observations. *Bull. Amer. Meteor. Soc.,* **82,** 889–901.

Houston, A. L., and R. B. Wilhelmson, 2007a: Observational analysis of the 27 May 1997 central Texas tornadic event. Part I: Prestorm environment and storm maintenance/propagation. *Mon. Wea. Rev.,* **135,** 701–726.

——, and ——, 2007b: Observational analysis of the 27 May 1997 central Texas tornadic event. Part II: Tornadoes. *Mon. Wea. Rev.,* **135,** 727–735.

——, and ——, 2012: The impact of airmass boundaries on the propagation of deep convection: A modeling-based study in a high-CAPE, low-shear environment. *Mon. Wea. Rev.,* **140,** 167–183.

Kalinowski, N. B., 2009: Unmanned aircraft operations in the National Airspace System. FAA Air Traffic Organization Policy N JO 7110.512. [Available online at www.faa.gov/documentLibrary/media/Notice/N7110.512.pdf.]

Lee, B. D., and R. B. Wilhelmson, 1997: The numerical simulation of nonsupercell tornadogenesis. Part II: Evolution of a family of tornadoes along a weak outflow boundary. *J. Atmos. Sci.,* **54,** 2387–2415.

Lin, P.-H., 2006: The first successful typhoon eyewall-penetration reconnaissance flight mission conducted by the unmanned aerial vehicle, Aerosonde. *Bull. Amer. Meteor. Soc.,* **87,** 1481–1483.

Mach, D. M., R. J. Blakeslee, J. C. Bailey, W. M. Farrell, R. A. Goldberg, M. D. Desch, and J. G. Houser, 2005: Lightning optical pulse statistics from storm overflights during the Altus Cumulus Electrification Study. *Atmos. Res.,* **76,** 386–401.

Maddox, R. A., L. R. Hoxit, and C. F. Chappell, 1980: A study of tornadic thunderstorm interactions with thermal boundaries. *Mon. Wea. Rev.,* **108,** 322–336.

Markowski, P. M., E. N. Rasmussen, and J. M. Straka, 1998: The occurrence of tornadoes in supercells interacting with boundaries during VORTEX-95. *Wea. Forecasting,* **13,** 852–859.

National Research Council, 2007: *Earth Science and Applications from Space: National Imperatives for the Next Decade and Beyond*. National Academies Press, 456 pp.

Newton, C. W., 1963: Dynamics of severe convective storms. *Severe Local Storms, Meteor. Mongr.,* No. 27, Amer. Meteor. Soc., 33–58.

NOAA, 2008: NOAA Budget Office, FY 2008 Blue Book (Budget Summary). [Available online at www.corporateservices.noaa.gov/nbo/08bluebook_highlights.html.]

Purdom, J. F. W., 1976: Some uses of high-resolution GOES imagery in the mesoscale forecasting of convection and its behavior. *Mon. Wea. Rev.,* **104,** 1474–1483.

——, 1993: Satellite observations of tornadic thunderstorms. *The Tornado: Its Structure, Dynamics, Prediction, and Hazards, Geophys. Monogr.,* Vol. 79, Amer. Geophys. Union, 265–274.

Ramanathan, V., M. V. Ramana, G. Roberts, D. Kim, C. Corrigan, C. Chung, and D. Winker, 2007: Warming trends in Asia amplified by brown cloud solar absorption. *Nature,* **448,** 575–579.

Rasmussen, E. N., S. Richardson, J. M. Straka, P. M. Markowski, and D. O. Blanchard, 2000: The association of significant tornadoes with a baroclinic boundary on 2 June 1995. *Mon. Wea. Rev.,* **128,** 174–191.

Schafer, R., P. T. May, T. D. Keenan, K. McGuffie, W. L. Ecklund, P. E. Johnston, and K. S. Gage, 2001: Boundary layer development over a tropical island during the Maritime Continent Thunderstorm Experiment. *J. Atmos. Sci.,* **58,** 2163–2179.

Simpson, J., B. R. Morton, M. C. McCumber, and R. S. Penc, 1986: Observations and mechanisms of GATE waterspouts. *J. Atmos. Sci.,* **43,** 753–782.

Stephens, G. L., and Coauthors, 2000: The Department of Energy's Atmospheric Radiation Measurement (ARM) Unmanned Aerospace Vehicle (UAV) program. *Bull. Amer. Meteor. Soc.,* **81,** 2915–2937.

van den Kroonenberg, A., T. Martin, M. Buschmann, J. Bange, and P. Vorsmann, 2008: Measuring the wind vector using the autonomous Mini Aerial Vehicle M^{2}AV. *J. Atmos. Oceanic Technol.,* **25,** 1969–1982.

van Vuren, R. J., 1981: Model aircraft operating standards. FAA Advisory Circular 91–57. [Available online at www.eoss.org/faa/ac91-57.pdf.]

Weaver, J. F., 1979: Storm motion as related to boundary-layer convergence. *Mon. Wea. Rev.,* **107,** 612–619.

——, and S. P. Nelson, 1982: Multiscale aspects of thunderstorm gust fronts and their effects on subsequent storm development. *Mon. Wea. Rev.,* **110,** 707–718.

Weckwerth, T. M., and D. B. Parsons, 2006: A review of convection initiation and motivation for IHOP_2002. *Mon. Wea. Rev.,* **134,** 5–22.

Wegener, S. S., B. Cobleigh, G. Buoni, and P. Hall, 2008: Western States Fire Mission; Ikhana, the COA and mission planning. Preprints, 12th Biennial USDA Forest Service Remote Sensing Applications Conf., Salt Lake City, UT, USDA. [Available online at http://svinetfc4.fs.fed.us/RS2008/s_wegener/index.htm.]

Wilhelmson, R. B., and C.-S. Chen, 1982: A simulation of the development of successive cells along a cold outflow boundary. *J. Atmos. Sci.,* **39,** 1466–1483.

Wilson, J. W., and W. E. Schreiber, 1986: Initiation of convective storms at radar-observed boundary-layer convergence lines. *Mon. Wea. Rev.,* **114,** 2516–2536.

——, T. M. Weckwerth, J. Vivekanandan, R. M. Wakimoto, and R. W. Russell, 1994: Boundary layer clear-air radar echoes: Origin of echoes and accuracy of derived winds. *J. Atmos. Oceanic Technol.,* **11,** 1184–1206.